JOURNAL OF SPACECRAFT AND ROCKETS
Vol. 32, No. 1, January–February 1995

Integrated Design of Hypersonic Waveriders Including Inlets and Tailfins

Sheam-Chyun Lin* and Yu-Shan Luo†
National Taiwan Institute of Technology, Taipei, Taiwan 10772, Republic of China

A generic aerospace vehicle including an airframe, inlet, and tail-wings, is developed by means of the waverider concept in this paper. The stream surfaces of the hypersonic flow past a cone with both transverse and longitudinal curvatures are used to design the forebody configuration. By suitably choosing the even polynomial stream surfaces, the airframe, horizontal stabilizers, and inlet can be constructed together. In addition, several small caret-waveriders are patched on this configuration as the vertical fins for the furnishment of a hypersonic vehicle. Also calculated are the mass flow rate, lift, drag, and lift-to-drag ratio. Moreover, effects of the various parameters on the shape and aerodynamic performance of this high-speed vehicle are found and discussed in detail. Hence, an overall aerodynamic design of a hypersonic vehicle is established in a simple and systematic way.

Nomenclature

a = speed of sound
G_{mn} = shock-perturbation factor
ℓ = length of right circular cone
ℓ_w = length of waverider
q = dynamic pressure, $\rho_\infty V_\infty^2/2$
R = distance quantities, $r\theta/\ell\delta$
r, θ, ϕ = spherical coordinate system
s = specific entropy
U, V, W = spherical velocity components perturbation associated with curvature
u, v, w = velocity components in spherical coordinates
X, Y = nondimensional cartesian coordinate system, $x/\ell\delta$, $y/\ell\delta$
x, y, z = Cartesian coordinate system
β = semivertex angle of the unperturbed shock
δ = semivertex angle of the unperturbed cone body
ϵ = perturbation parameter (defined as extremely small)
σ = ratio of shock angle to cone semivertex angle, β/δ

Subscripts

c = compression surface quantities
F = forebody quantities
f = freestream surface quantities
fin = tailfin quantities
i = inlet surface quantities
L = inlet left side quantities
ℓ = shock wave in base plane
m = mth term in expansion
n = nth term in expansion
o = zero-order, unperturbed flow quantities
R = inlet right side quantities
s = shock wave
w = waverider surface quantities
∞ = freestream condition

Superscripts

$*$ = quantities proposed in Ref. 8

Received May 17, 1993; revision received Oct. 4, 1993; accepted for publication Oct. 12, 1993.

*Associate Professor, Department of Mechanical Engineering. Member AIAA.
†Graduate Research Assistant, Department of Mechanical Engineering.

Introduction

IN recent years, substantial potential demand for a high-speed civil transport (HSCT) has generated renewed interests in high-speed and high-lift aerodynamics. Modern design philosophy shows that a highly integrated configuration including the blending of an airframe, propulsion unit, and wings usually results in an aerodynamically efficient design. The complex flowfield around such a highly integrated configuration is usually too complicated to analyze adequately and accurately, even using advanced computational fluid dynamics (CFD) methods. Hence, the establishment and refinement of simplified calculation schemes appropriate for the design of blended configurations are highly desirable.

One attractive approach for studying the properties of blended lifting bodies is that of waverider aerodynamics. The aerodynamic advantage of the waverider is that the high pressure behind the shock wave under the vehicle does not "leak" around the leading edge to the top surface, so that the lift-to-drag ratio (L/D) for the waverider is considerably higher than that for the conventional aerodynamic vehicle. Moreover, waveriders yield flowfields and aerodynamic properties that are accurately known for their particular on-design conditions. Thus, they provide reliable baseline results for a wide range of Mach numbers and configuration geometries and allow for the systematic variation of parameters that are pertinent to the design process.

Because of the concept of construction,[1] the waverider configurations available are the caret waverider[2] and the cone-derived waverider,[3] for which the exact flowfield solution exists. The major research efforts are focused on the cone-derived waverider for its superior performance and volumetric advantage over the caret waverider. Although such configurations are not new, the nonanalytical and numerically tabulated nature of the flowfield variables rendered parametric studies impractical for design considerations. In 1980, however, Rasmussen[4] utilized an approximate analytical solution, in the framework of hypersonic small-disturbance theory, together with perturbation methods to generate a wide class of waverider configurations stemming from both axisymmetric and nonaxisymmetric conical flows. This analytical approach led to a number of papers dealing with optimization, viscous effects, and systematic construction schemes.[5–7] The generalization of this approach for arbitrary small conical perturbations of the flow past a cone with combined transverse and longitudinal curvature was derived by Lin and Rasmussen,[8] and they also demonstrated an increase of the lift-to-drag ratio.

Besides the forebody considered in the above works, following the underlying principle used in the design of a waverider itself, Hemdan and Jischke[9] took the stream surface of the flowfield for the elliptic cone as a solid surface, assumed inviscid flow, and proceeded to design smooth blended inlets attached to the waverider

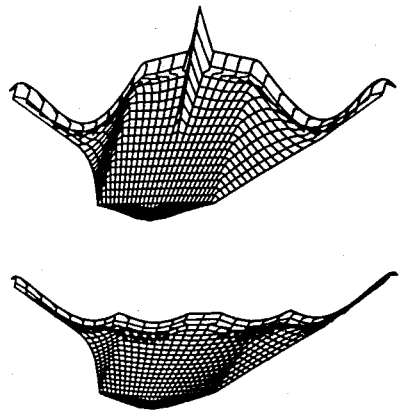

Fig. 1 Upper and lower surfaces of the whole body.

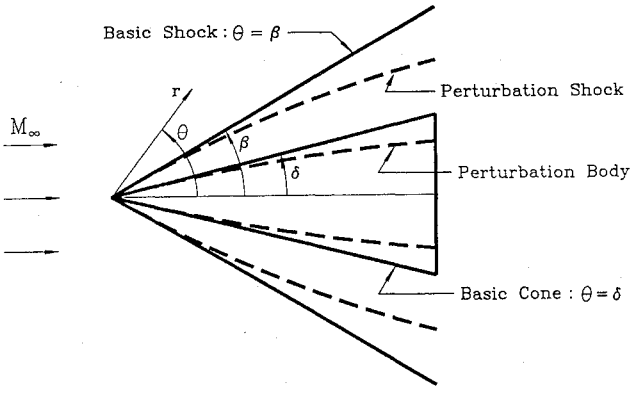

Fig. 2 Nonconical body produced by perturbation of a cone.

configuration. However, their work was still far from practical application because of the lack of complete analytical analysis of aerodynamic parameters. Following and extending this idea, Lin and Luo[10] generated the integrated inlet for the waverider with combined transverse and longitudinal curvature. Their work includes the analytical expressions of many aerodynamic characteristics and an extensive parametric study.

Until now, no attempt has been made to design a generic aerospace vehicle including an airframe, horizontal stabilizer, vertical fins, and twin-inlet by waverider concepts. In this paper, a reflexed trailing edge polynomial together with the approximate analytic solution[8] is utilized to generate a forebody configuration with horizontal stabilizers. A suitable choice of a second-order polynomial is used to design the integrated twin-inlet. Several small caret waveriders are then patched on the forebody to furnish this hypersonic vehicle. Using the superposition method, the mass flow rates, lift, drag, and lift-to-drag ratio can be derived and expressed in a closed form. Thus, not only the whole configuration of a high-speed vehicle (see Fig. 1) is designed in a simple and systematic way, but also many aerodynamic effects of the various parameters on the shapes of each portion for this vehicle are calculated and studied.

Airframe and Horizontal Stabilizer Generation

Perturbation Flowfield

In spherical coordinates, as shown in Fig. 2, the pointed body with combined transverse and longitudinal curvature is represented by

$$\theta = \delta[1 - \epsilon(r/\ell)^m \cos(n\phi)] \tag{1}$$

The transverse curvature is introduced by $\cos(n\phi)$ of which n is an integer, and $(r/\ell)^m$ is a function that produces the longitudinal curvature. It follows that the various flowfield variables are expanded in power of ϵ as (see Ref. 8 for details)

$$\theta = \theta_o + \epsilon\theta_{mn}(\theta_o)(r/\ell)^m \cos(n\phi) \tag{2}$$

$$u(r, \theta_o, \phi) = u_o(\theta_o) + \epsilon U_{mn}(\theta_o)(r/\ell)^m \cos(n\phi) + \mathcal{O}(\epsilon^2)$$

$$v(r, \theta_o, \phi) = v_o(\theta_o) + \epsilon V_{mn}(\theta_o)(r/\ell)^m \cos(n\phi) + \mathcal{O}(\epsilon^2) \tag{3}$$

$$s(r, \theta_o, \phi) = s_o + C_v\epsilon S_{mn}(\theta_o)(r/\ell)^m \cos(n\phi) + \mathcal{O}(\epsilon^2)$$

The basic conical flow variables u_o, v_o, and s_o can be obtained from the hypersonic small disturbance theory.[4] The outer expansions (2) and (3) are substituted into the governing equations. Also the new variables U^*_{mn}, V^*_{mn}, and U^{**}_{mn} are introduced to simplify these equations so that

$$U_{mn} = U^*_{mn} + \theta_{mn} v_o$$

$$V_{mn} = V^*_{mn} + \theta_{mn}\frac{\mathrm{d}v_o}{\mathrm{d}\theta_o} \tag{4}$$

$$U^{**}_{mn} = U^*_{mn} + \frac{a_o^2 S_{mn}}{\gamma(\gamma - 1)u_o}$$

Finally, the general solution is attained as

$$\frac{U^{**}_{mn}(\zeta)}{V_\infty \delta^2} = I_n(\lambda_m\zeta)G_{mn}[A_{mn} + X_{mn}(\zeta)] + K_n(\lambda_m\zeta)G_{mn}[B_{mn} - Y_{mn}(\zeta)] \tag{5}$$

where I_n and K_n are, respectively, the first and second kind modified Bessel functions, and

$$X_{mn}(\zeta) = n^2(1+m)\sigma(\xi_o - 1)^2 \int_1^\zeta \frac{K_n(\lambda_m\zeta)}{\zeta}\left(\frac{1}{I}\right)^{1+m} \mathrm{d}\zeta$$

$$Y_{mn}(\zeta) = n^2(1+m)\sigma(\xi_o - 1)^2 \int_1^\zeta \frac{I_n(\lambda_m\zeta)}{\zeta}\left(\frac{1}{I}\right)^{1+m} \mathrm{d}\zeta$$

$$\zeta = \theta_o/\delta$$

$$I = \exp\left[\int_\beta^{\theta_o} \frac{u_o}{v_o}\mathrm{d}\theta_o\right]$$

$$A_{mn} = N_{mn} - X_{mn}(\sigma)$$

$$B_{mn} = Q_{mn} - Y_{mn}(\sigma)$$

$$G_{mn} = \frac{1+m}{R_{mn}}\frac{V^*_{mn}(\zeta = 1)}{V_\infty \delta}$$

$$N_{mn} = \frac{(1+m)\sigma}{G_{mn}} \times \left[K_n(\lambda_m\sigma)\frac{V^*_{mn}(\sigma)}{V_\infty\delta} - \frac{\lambda_m}{1+m}K'_n(\lambda_m\sigma)\frac{U^{**}_{mn}(\sigma)}{V_\infty\delta^2}\right]$$

$$Q_{mn} = \frac{1}{K_n(\lambda_m\sigma)G_{mn}}\frac{U^{**}_{mn}(\sigma)}{V_\infty\delta^2} - \frac{[I_n(\lambda_m\sigma)]}{K_n(\lambda_m\sigma)}N_{mn}$$

$$R_{mn} = \lambda_m[I'_n(\lambda_m)A_{mn} + K'_n(\lambda_m)B_{mn}]$$

Body Generation

A nonconical waverider configuration can be constructed by specifying either the trailing edge of the compression surface in the base plane, or by specifying the trailing edge of the freestream surface in the base plane. (The waveriders considered here all have upper surfaces parallel to the freestream.) Assume that the curve for the compression trailing edge is specified. Then the shock-layer streamlines passing through this base curve can be traced upstream to where they intersect the conical shock (i.e., from point B to point C in Fig. 3). These streamlines lie in a stream surface that constitutes the compression surface of a new waverider configuration. The conical flowfield above the intersection line can now be discarded and replaced by a new freestream surface constructed by tracing undisturbed freestream streamlines downstream from the shock-intersection line (from point C to point A in Fig. 3). These streamlines constitute

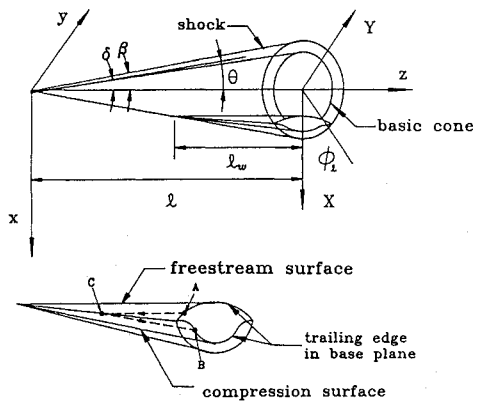

Fig. 3 Geometric configuration and coordinate system.

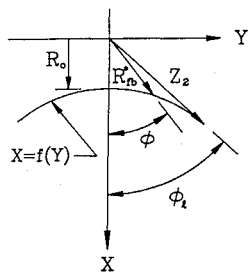

Fig. 4 Nondimensional coordinate system in the base plane.

the new freestream surface of the waverider. This freestream surface intersects the base plane and forms a freestream trailing-edge curve. Thus, specifying the compression surface trailing-edge curve in the base plane automatically determines the freestream surface trailing-edge in the base plane. The reverse process is also valid; and this reverse approach is more convenient for the purpose of this analysis.

To simplify the analysis, cones with small semivertex angles are considered so that the nondimensional coordinates are $X = x/(\ell\delta)$ and $Y = y/(\ell\delta)$ (see Fig. 4). The waverider freestream trailing-edge curve in the base plane is described by a function of the form $X = X(Y)$, which, with some generality, can be specified by the sixth-order even polynomial

$$X = R_o + b_2 Y^2 + b_4 Y^4 + b_6 Y^6 \tag{6}$$

As proposed in Ref. 7, the trailing-edge curves that have two minimums and one maximum are chosen to generate the waverider shape with horizontal stabilizer. One minimum is at the symmetry plane $Y = 0$. Let Y_1 be the location of the maximum of $X(Y)$, Y_2 be the location of the second minimum, and $Y_2 > Y_1$. So, the coefficients b_2, b_4, and b_6 are specified by

$$\begin{aligned} b_2 &= 3\omega_1^2\omega_2^2 Y_{\phi_\ell}^4 b_6 \\ b_4 &= -3\left(\omega_1^2 + \omega_2^2\right) Y_{\phi_\ell}^2 b_6/2 \\ b_6 &= \frac{(X_{\phi_\ell} - R_o)/Y_{\phi_\ell}^6}{1 + 3\omega_1^2\omega_2^2 - 3\left(\omega_1^2 + \omega_2^2\right)/2} \end{aligned} \tag{7}$$

where $\omega_1 \equiv Y_1/Y_{\phi_\ell}$ and $\omega_2 \equiv Y_2/Y_{\phi_\ell}$.

To illustrate the effects for the attachments of inlet and vertical fins, it is necessary to consider a particular forebody (see Fig. 5) with the following design conditions: $M_\infty = 10$, $\delta = 8$ deg; $\epsilon = 0.1$; $m = 1$; $n = 2$; $\phi_\ell = 50$ deg; $R_o = X_{\phi_\ell}/2$; $\omega_1 = 0.62$; and $\omega_2 = 0.94$. In addition, to smooth the affiliation of vertical fins, a plate freestream surface ($X = X_{\text{fin}}$) is picked to replace the original freestream surface in the region $0 \le Y \le Y_{\text{fin}}$, as shown in Fig. 6 ($Y_{\text{fin}}/Y_{\phi_\ell} = 0.3$). Obviously, the available location for vertical fins can be varied by different values of Y_{fin}.

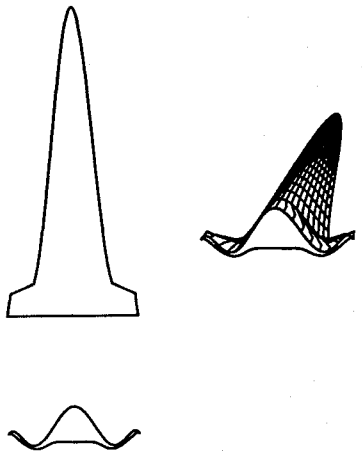

Fig. 5 Reflexed trailing edge waverider with curvature.

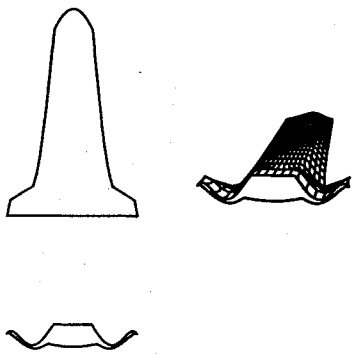

Fig. 6 Waverider forebody with partial flat-plate freestream surface.

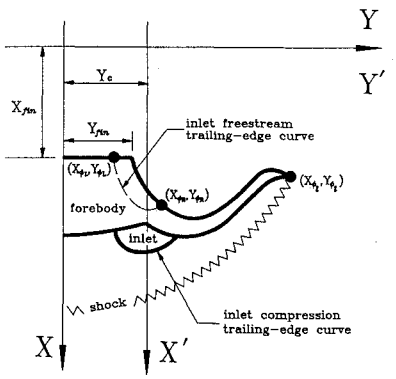

Fig. 7 Inlet geometric back view.

Inlet Considerations

To simplify the analysis, an infinitesimally thin inlet wall is considered here. Its presence, therefore, will not affect the flowfield; i.e., the flow will tend to move easily past the inlet without producing any disturbance. Following the aforementioned approach used to develop the waverider configuration for a framebody, the inlet will be constructed from the same flowfield. Also, air flowing through the stream tube, confined by the waverider and the inlet compression stream surfaces, will be the oncoming flow for the propulsion unit.

A second-order even polynomial is used to specify the inlet freestream trailing-edge curve in the base plane (see Fig. 7)

$$X' = R_{io} + b_{i2} Y'^2 \tag{8}$$

The X', Y' coordinates can be translated to the X, Y coordinates by the relationship $X' = X$ and $Y' = Y - Y_c$. It follows that the inlet freestream trailing-edge curve can be rewritten as

$$X = R_{io} + b_{i2}(Y - Y_c)^2 \tag{9}$$

It is useful to introduce two parameters ϕ_R and ϕ_L to specify the right and left limits of the inlet. Also, to obtain the stream tube of the inlet, both the waverider freestream trailing-edge curve and the inlet trailing-edge curve must pass through the points (X_{ϕ_R}, Y_{ϕ_R}) and (X_{ϕ_L}, Y_{ϕ_L}) when $\phi = \phi_R$ and $\phi = \phi_L$, respectively. Therefore, the conditions below must be satisfied

$$X_{w\phi_R} = X_{i\phi_R} \qquad Y_{w\phi_R} = Y_{i\phi_R} \qquad X_{w\phi_L} = X_{i\phi_L} \tag{10}$$

$$Y_{w\phi_L} = Y_{i\phi_L} \tag{11}$$

where subscripts w and i represent the properties of the waverider and the inlet, respectively. After some algebraic calculations, it is easy to show that

$$Y_c = \frac{X_L - X_R}{2b_{i2}(Y_R - Y_L)} + \frac{Y_R + Y_L}{2} \tag{12}$$

In summary, parameter R_{io} is specified to control the inlet thickness and the position and width of an inlet are designated by the two variables ϕ_R and ϕ_L.

Because the inlet length depends on the length of the propulsion unit, it is not necessary to take the whole inlet compression surface; i.e., from shock-intersection line to base plane, as the inlet wall. To control the inlet length, the fractional parameter (r_i/ℓ) is chosen in the following analyses. Physically speaking, the region $(r_i/\ell) \geq (r/\ell)$ is utilized as the actual inlet wall, while the front portion of the inlet compression surface is discarded.

Vertical Fin Geometry

As stated previously, the caret-waverider derived from a two-dimensional flow past an infinite wedge is used as the vertical fins. A typical caret-waverider is shown in Fig. 8. The relation between wedge angle δ_{fin} and shock angle β_{fin} is obtained as

$$\tan\delta_{\text{fin}} = \cot\beta_{\text{fin}} \frac{M_\infty^2 \sin^2\beta_{\text{fin}} - 1}{1 + \{[(\gamma+1)/2] - \sin^2\beta_{\text{in}}\}M_\infty^2} \tag{13}$$

With the aid of hypersonic small-disturbance approximation,[11] the preceding relation can be rewritten in the form

$$\frac{\sin\beta_{\text{fin}}}{\sin\delta_{\text{fin}}} = \frac{\gamma+1}{4} + \sqrt{\left(\frac{\gamma+1}{4}\right)^2 + \frac{1}{M_\infty^2 \sin^2\delta_{\text{fin}}}} \tag{14}$$

Also, the length of the vertical fin is expressed as

$$\ell_{\text{fin}} = W_{\text{fin}}/[2\sin\beta_{\text{fin}}\tan(\phi_{\text{fin}}/2)] \tag{15}$$

As mentioned in the previous section, the upper surface of the forebody is replaced by a plate freestream surface in region $0 \leq Y \leq Y_{\text{fin}}$, so it is easy to place two caret-waveriders on the upper surface; thereafter, a forebody with vertical fins is constructed. The controlling parameters of its position and shape are demonstrated in Fig. 9. Note that these two fins will merge into one vertical fin for the case: $s_{\text{fin}} = Y_{\text{fin}}$ and $\phi_{\text{fin}} = \pi/2$.

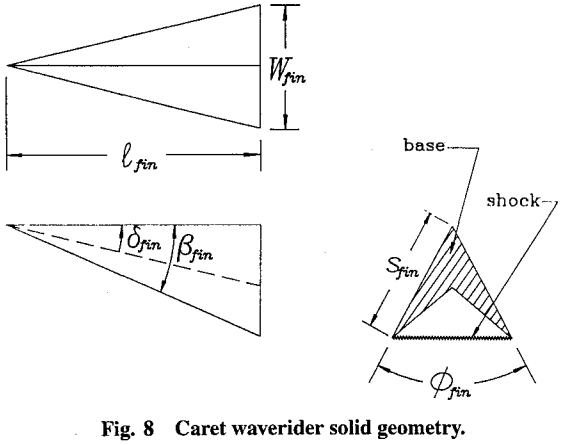

Fig. 8 Caret waverider solid geometry.

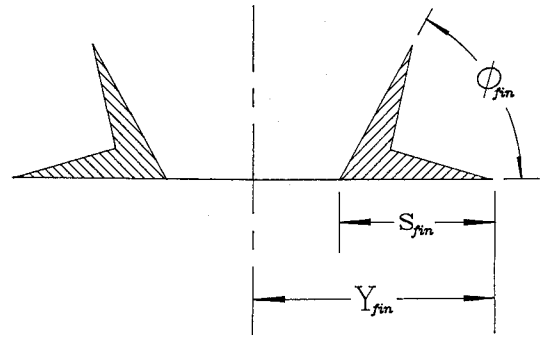

Fig. 9 Vertical fins geometry.

Aerodynamic Performance

Mass Flow Rate of Inlet

In principle, the mass flow rate will be given by

$$\text{mass flow rate} = \int\int \rho V \cdot \mathrm{d}A \tag{16}$$

As derived in Ref. 8, the analytic approximate expressions for density and velocity inside the shock-layer are very complicated, so the integration of Eq. (16) is intractable. To avoid this difficulty, a simple alternative proposed in Ref. 10 is adopted in this paper. As discussed earlier, the inlet portion confined by the compression stream surfaces of the waverider and inlet wall can be treated as a stream tube, and thus the mass flow rate of this stream tube is tantamount to the mass flow rate of the inlet. Because of the definition of stream surfaces, the identical mass flow rate can be obtained in any cross section of this stream tube.

Obviously, the desirable location should be selected in a freestream region where the density and velocity are kept as constant values. To achieve this, we extend this stream tube forward to where it intersects with the shock, and evaluate the mass flow rate over that particular cross section (see section A_{if} in Fig. 10). Therefore, the mass flow rate is easily obtained as the product of the cross section area A_{if}, freestream density, and velocity

$$\text{mass flow rate} = \rho_\infty V_\infty A_{if} \tag{17}$$

Note that the direction of this cross section area A_{if} is in parallel with the freestream flowfield. Furthermore, according to the construction principle of waveriders, the freestream and compression stream surfaces share the same leading edge, which is the intersection line of shock and stream tube; it follows that the lower curve of A_{if} can be replaced by the leading edge of the inlet freestream surface. Therefore, the projection of cross section A_{if} on the base plane will be the area A confined by the freestream trailing-edge curve of the waverider and the inlet, as shown in Fig. 10.

In conclusion, with the aid of the freestream trailing-edge curve for the waverider and inlet, the useful cross-section area of the stream tube can be expressed as

$$A = A_{if} = 2\int_{Y_{\phi_L}}^{Y_{\phi_R}} (X_w - X_i)\,\mathrm{d}Y \tag{18}$$

For convenience, a nondimensional mass flow rate parameter is defined as

$$\dot{m} = \frac{\text{mass flow rate}}{\rho_\infty V_\infty \ell_w^2} \tag{19}$$

Lift-to-Drag Ratio

Lift and drag of the waverider configurations can be obtained by means of the integral momentum equations for inviscid flow.[11] This process reduces the formulas for lift L and wave drag D_w to area integrals over the shock-layer area between the body and shock in the base plane. Recall that the complete vehicle configuration

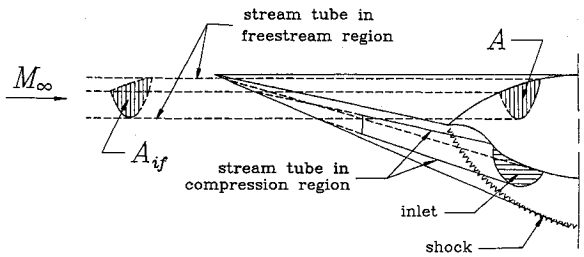

Fig. 10 Inlet stream tube side view.

is composed of two sections—the forebody and the vertical fins. For this complete vehicle configuration (only the afterbody is not included), these expressions are related to a cone-derived waverider and are expressed as (see Ref. 10 for details)

$$L_F = 4q\ell^2\delta^2\Bigg[\int_{\phi_R}^{\phi_\ell}\int_{\theta_{cb}}^{\beta} F1(\theta_o,\phi)\,\mathrm{d}\theta_o\,\mathrm{d}\phi + \int_{\phi_L}^{\phi_R}\int_{\theta_{icb}}^{\beta} F1(\theta_o,\phi)\,\mathrm{d}\theta_o\,\mathrm{d}\phi + \int_{0}^{\phi_L}\int_{\theta_{cb}}^{\beta} F1(\theta_o,\phi)\,\mathrm{d}\theta_o\,\mathrm{d}\phi + (r_i/\ell)^2\Bigg(\int_{\phi_L}^{\phi_R}\int_{\theta_{cb}}^{\beta} F1(\theta_o,\phi)\,\mathrm{d}\theta_o\,\mathrm{d}\phi - \int_{\phi_L}^{\phi_R}\int_{\theta_{icb}}^{\beta} F1(\theta_o,\phi)\,\mathrm{d}\theta_o\,\mathrm{d}\phi\Bigg)\Bigg] \tag{20}$$

$$D_{wF} = 2q\ell^2\delta^2\Bigg[\int_{\phi_R}^{\phi_\ell}\int_{\theta_{cb}}^{\beta} F2(\theta_o,\phi)\,\mathrm{d}\theta_o\,\mathrm{d}\phi + \int_{\phi_L}^{\phi_R}\int_{\theta_{icb}}^{\beta} F2(\theta_o,\phi)\,\mathrm{d}\theta_o\,\mathrm{d}\phi + \int_{0}^{\phi_L}\int_{\theta_{cb}}^{\beta} F2(\theta_o,\phi)\,\mathrm{d}\theta_o\,\mathrm{d}\phi + (r_i/\ell)^2\Bigg(\int_{\phi_L}^{\phi_R}\int_{\theta_{cb}}^{\beta} F2(\theta_o,\phi)\,\mathrm{d}\theta_o\,\mathrm{d}\phi - \int_{\phi_L}^{\phi_R}\int_{\theta_{icb}}^{\beta} F2(\theta_o,\phi)\,\mathrm{d}\theta_o\,\mathrm{d}\phi\Bigg)\Bigg] \tag{21}$$

where

$$F1(\theta_o,\phi) = \frac{\rho(\beta)}{\rho_\infty}\cos(\phi) + \epsilon L^*_{mn}$$

$$F2(\theta_o,\phi) = \left[\frac{\rho(\beta)}{\rho_\infty}\left(2 + \ell_n\left(\frac{\beta^2}{\theta_o^2}\right) - \frac{C_{p_o}}{\delta^2} + \epsilon D^*_{mn}\cos(n\phi)\right)\right]\theta_o$$

$$L^*_{mn} = \left[\rho_{mn} + \frac{\mathrm{d}\theta_{mn}}{\mathrm{d}\theta_o} + \frac{\theta_{mn}}{\theta_o} + \frac{\theta_o}{\delta}\left(\frac{\theta_{mn}}{\delta} + \frac{V_{mn}}{V_\infty\delta}\right)\right] \times \cos(\phi)\cos(n\phi) - \frac{\theta_o}{\delta}\frac{W_{mn}}{V_\infty\delta}\sin(\phi)\sin(n\phi)$$

$$D^*_{mn} = \left[\frac{\rho_o}{\rho_\infty}\left(2 + \ell_n\frac{\beta^2}{\theta_o^2}\right) - \frac{C_{p_o}}{2}\right]\left[\frac{\theta_{mn}}{\theta_o} + \frac{\mathrm{d}\theta_{mn}}{\mathrm{d}\theta_o}\right] + \frac{\rho_o}{\rho_\infty}\left[\rho_{mn}\left(2 + \ell_n\frac{\beta^2}{\theta_o^2}\right) - 2\left(\frac{U_{mn}}{V_\infty\delta^2} - \frac{\theta_{mn}}{\theta_o} - 2\frac{V_{mn}}{V_\infty\delta}\frac{\theta_o}{\delta}\right)\right] - \frac{C_{p_{mn}}}{\delta^2}$$

In the second part, caret waveriders are utilized as the vertical fins. Thus, the lift and wave drag are given by

$$L_{\text{fin}} = 2\left[\frac{2qW_{\text{fin}}\ell_{\text{fin}}}{M_\infty^2(\gamma+1)}\left(M_\infty^2\sin^2\beta_{\text{fin}} - 1\right)\right] \tag{22}$$

$$D_{w\text{fin}} = L_{\text{fin}}\tan\delta_{\text{fin}} \tag{23}$$

To calculate the total lift and drag of the whole configuration, the quantities associated with the preceding two portions should be summed together to yield

$$L = L_F - L_{\text{fin}}\sin\phi_{\text{fin}}/2 \tag{24}$$

$$D_w = D_{wF} + D_{w\text{fin}} \tag{25}$$

The total drag is determined by

$$D = D_w + D_f + D_b \tag{26}$$

Here, D_w is the inviscid wave drag on the forebody. The friction drag D_f is represented by qC_fS_w, where S_w is the forebody wetted area, and C_f is an average skin-friction coefficient. Here, $C_f = 0.001$ was chosen for the parametric study in the next section. The base drag D_b is ignored and set to zero in the subsequent analysis (this is tantamount to assuming that the base pressure is P_∞).

With regard to the total wetted area S_w of the forebody, it is determined by the geometry of the waverider and can be expressed as

$$S_w = S_{wu} + S_{wl} \tag{27}$$

where the upper wetted area S_{wu} is specified as

$$S_{wu} = 2\ell^2\delta\int_0^{\phi_s}\sigma[1-Z]\left[Z^2 + \frac{R_{cb}^2R_{cb}'^2}{\left(R_{cb}^2-1\right)(\sigma^2-1)}\right]^{1/2}\mathrm{d}\phi + 2\ell_{\text{fin}}^2\sqrt{(\beta_{\text{fin}}-\delta_{\text{fin}})^2 + \beta_{\text{fin}}^2\tan^2(\phi_{\text{fin}}/2)} \tag{28}$$

and the lower wetted area S_{wl} is given by

$$S_{wl} = 2\ell^2\delta\Bigg(\int_{\phi_R}^{\phi_\ell}\int_Z^1\left[\frac{R_{cb}^2R_{cb}'^2}{R_{cb}^2-1+X} + R_{cb}^2 - 1 + X^2\right]^{1/2}\mathrm{d}X\,\mathrm{d}\phi + \int_{\phi_L}^{\phi_R}\int_{Z_i}^1\left[\frac{R_{icb}^2R_{icb}'^2}{R_{icb}^2-1+X} + R_{icb}^2 - 1 + X^2\right]^{1/2}\mathrm{d}X\,\mathrm{d}\phi + \int_0^{\phi_L}\int_Z^1\left[\frac{R_{icb}^2R_{icb}'^2}{R_{icb}^2-1+X} + R_{icb}^2 - 1 + X^2\right]^{1/2}\mathrm{d}X\,\mathrm{d}\phi + \int_{\phi_L}^{\phi_R}\int_Z^{r_i/\ell}\left[\frac{R_{cb}^2R_{cb}'^2}{R_{cb}^2-1+X} + R_{cb}^2 - 1 + X^2\right]^{1/2}\mathrm{d}X\,\mathrm{d}\phi - \int_{\phi_L}^{\phi_R}\int_{Z_i}^{r_i/\ell}\left[\frac{R_{icb}^2R_{icb}'^2}{R_{icb}^2-1+X} + R_{icb}^2 - 1 + X^2\right]^{1/2}\mathrm{d}X\,\mathrm{d}\phi\Bigg) \tag{29}$$

where

$$Z = \left(\frac{R_{cb}^2-1}{\sigma^2-1}\right)^{1/2}$$

$$Z_i = \left(\frac{R_{icb}^2-1}{\sigma^2-1}\right)^{1/2}$$

Parametric Analysis

Parametric analyses are performed to determine the aerodynamic characteristics influenced by the additions of inlet and vertical fins. To illustrate the parametric study, a particular forebody configuration with horizontal stabilizers is considered; it is constructed of a sixth-order freestream trailing-edge curve with reflexed trailing edge and with the following design conditions: $M_\infty = 10$; $\delta = 8$ deg; $\phi_\ell = 50$ deg; $R_o = X_{\phi_\ell}/2$; $m = 1$; $n = 2$; $\epsilon = 0.1$; $w_1 = 0.62$; $w_2 = 0.94$; $Y_{\text{fin}}/Y_{\phi_\ell} = 0.3$. This type of waverider configuration has been extensively discussed in Ref. 7.

The previous section has shown that four important parameters (R_{io}, ϕ_R, ϕ_L, r_i/ℓ) control the inlet shape. Also, there are three parameters (δ_{fin}, ϕ_{fin}, s_{fin}) for the variation of vertical-fins geometry. The influence of the parameters on the aerodynamic forces will be discussed in detail in the following subsections.

Influence of Inlets Added

The inlet thicknes is controlled directly by R_{io} (increasing R_{io} thickens the inlet). Moreover, the cross section area of an inlet enlarges with an increase in R_{io}. It follows that the mass flow rate of the inlet also increases with R_{io}. According to the characteristics of conical flow, the pressure is greater at the body than at the shock. Thus, increasing R_{io} results in decreasing pressure on the inlet wall and, consequently, both the lift and the wave drag will decrease. Conversely, the wetted area enlarges as the inlet shape thickens; thus, the friction drag D_f increases with R_{io}. In summary, the lift decreases more than the drag, which produces a decrease in L/D, as demonstrated in Table 1.

The cross section area and mass flow rate of an inlet become larger as ϕ_R increases or ϕ_L decreases. Similarly, the lift-to-drag ratio decreases as ϕ_R increases or ϕ_L decreases. The fraction parameter r_i/ℓ is designed to control the inlet length. Only the portion of $(r/\ell) \geq (r_i/\ell)$ is related to the inlet wall; thus, the inlet becomes shorter as r_i/ℓ increases. When r_i/ℓ reaches unity, the inlet unit disappears. From the foregoing discussion, the inlet portion can be treated as a stream tube; hence, a constant mass flow rate is expected and is independent of the length of the inlet. Note that this conclusion is only valid for an inviscid flow. Therefore, the variation of r_i/ℓ would not change the mass flow rate of the inlet. However, the increase of r_i/ℓ causes a shorter inlet section, which has smaller frictional drag. With the unchanged lift force, an increase in L/D is obtained for increasing r_i/ℓ. The results above also can be found in Table 1.

Table 1 Properties of waverider with inlet for various parameters

R_{io}	ϕ_L, deg	ϕ_R, deg	r_i/ℓ	$\dot{m}$	L/q	L/D
0.90	5	25	0.90	0.00495	0.09878	6.0923
0.95	5	25	0.90	0.00640	0.09800	6.0645
1.00	5	25	0.90	0.00783	0.09725	6.0357
0.90	0	25	0.90	0.00681	0.09814	6.0802
0.90	5	25	0.90	0.00495	0.09878	6.0923
0.90	10	25	0.90	0.00303	0.09943	6.1133
0.90	5	15	0.90	0.00316	0.10062	6.1242
0.90	5	20	0.90	0.00484	0.09999	6.1072
0.90	5	25	0.90	0.00495	0.09878	6.0923
0.90	5	25	0.90	0.00495	0.09878	6.0923
0.90	5	25	0.95	0.00495	0.10027	6.1328
0.90	5	25	1.00	0.00495	0.10183	6.1745

Table 2 Properties of waverider with inlet and vertical fins for various parameters

δ_{fin}, deg	ϕ_{fin}, deg	$s_{\text{fin}}/Y_{\text{fin}}$	L/q	D/q	L/D
1	60	2/3	0.09833	0.01680	5.8540
2	60	2/3	0.09786	0.01674	5.8467
3	60	2/3	0.09740	1.01674	5.8185
3	50	2/3	0.09775	0.01672	5.8448
3	60	2/3	0.09740	0.01674	5.8185
3	70	2/3	0.09707	0.01675	5.7957
3	60	1/3	0.09809	0.01638	5.9879
3	60	2/3	0.09740	0.01674	5.8185
3	60	1	0.09672	0.01729	5.5937

Table 3 Properties of waverider with single vertical fin or vertical flat plate

δ_{fin}	ϕ_{fin}	$s_{\text{fin}}/Y_{\text{fin}}$	L/q	D/q	L/D
1	90	1	0.09767	0.01733	5.6360
——	90	1	0.09878	0.01680	5.8790[a]
2	90	1	0.09654	0.01725	5.5970
——	90	1	0.09878	0.01674	5.8991[b]
3	90	1	0.09541	0.01726	5.5274
——	90	1	0.09878	0.01669	5.9170[c]

[a]Height and length of vertical flat plate are equal to $\delta_{\text{fin}} = 1$ deg case.
[b]Height and length of vertical flat plate are equal to $\delta_{\text{fin}} = 2$ deg case.
[c]Height and length of vertical flat plate are equal to $\delta_{\text{fin}} = 3$ deg case.

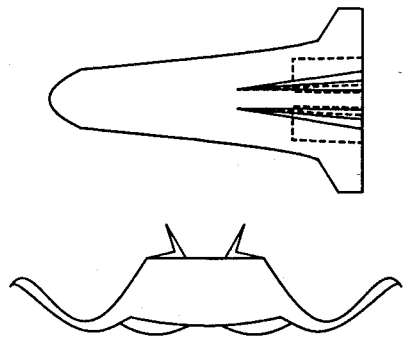

Fig. 11 Typical configration with combined inlets and vertical fins, top view and back view.

Influence of Vertical Fins Added

As described in Eqs. (24) and (25), the total lift and drag vary with the lift introduced by vertical fins (i.e., L_{fin}). Also, in principle, the lift vector of a caret waverider could be acting in a positive or negative direction for different attachments of vertical fins. For a reasonable simulation, as shown in Fig. 9, the total lift will decrease and total drag will increase when two caret waveriders are attached on the forebody as vertical fins. It follows that vertical fins have a negative influence on lift-to-drag ratio for the complete vehicle configuration. Also, it should be kept in mind that the lift of a caret waverider becomes larger as the size of the vertical fins enlarges (that is δ_{fin}, ϕ_{fin}, and s_{fin} increase). Conversely, the total lift and lift-to-drag ratio of the complete vehicle decrease with a larger vertical fin. Table 2 offers data to support these arguments (where $R_{io} = 0.9$; $\phi_R = 25$ deg; $\phi_L = 5$ deg; $r_i/\ell = 0.9$).

As mentioned in the previous section, two caret waveriders will merge into one vertical fin for $s_{\text{fin}} = Y_{\text{fin}}$ and $\phi_{\text{fin}} = 90$ deg. Then the geometry of the vertical fin is only dependent on the variation of wedge angle δ_{fin}. An increase of δ_{fin} causes a thickened caret-waverider vertical fin that results in a more negative effect on lift because of a stronger shock wave. This conclusion can be found in Table 3. Also, it is worthwhile to consider a flat plate for the vertical fin, which can be obtained when the thickness factor δ_{fin} mears zero. The wetted area (i.e., skin friction) would be added, while the lift would not be affected. Thus, the lift and lift-to-drag ratio will reach the maximum, as demonstrated in Table 3. Nevertheless, this flat-plat vertical fin might not be realistic from a practical point of view. Figure 11 presents a complete vehicle configuration designed in this study with the design conditions as: $R_{io} = 0.9$; $\phi_R = 25$ deg; $\phi_L = 5$ deg; $r_i/\ell = 0.9$; $\delta_{\text{fin}} = 3$ deg; $\phi_{\text{fin}} = 60$ deg; and $s_{\text{fin}}/Y_{\text{fin}} = 2/3$.

Concluding Remarks

A simple and systematic design scheme has been established in this study for a complete vehicle configuration including the frame-body, horizontal stabilizers, inlets, and vertical fins. The inlet is

attached to the waverider configuration and is positioned to capture a favorable flow into the engine; thus, the design of the inlet for the scramjet is simplified. The horizontal stabilizer and vertical fins are also constructed together for the completion of a generic aerospace vehicle. Furthermore, the design scheme offers an explicit, approximate, analytical form for both aerodynamic performance and geometric factors. These results can be used to perform systematic and parametric studies.

Acknowledgments

The financial support for this work from National Science Council Grant NSC 82-0424 E-011-013 is gratefully acknowledged.

References

[1]Kuchemann, D., "Waverider Aircraft," *The Aerodynamic Design of Aircraft*, 1st ed., Pergamon, Oxford, England, UK, 1978, pp. 448–510.

[2]Nonweiler, T. R. F., "Aerodynamic Problems of Manned Space Vehicles," *Royal Aeronautical Society Quarterly Journal*, Vol. 63, No. 585, 1959, pp. 521–528.

[3]Jones, J. G., "A Method for Designing Lifting Configurations for High Supersonic Speeds Using the Flow Fields of Nonlifting Cones," Aeronautical Research Council R&M 3539, March 1963.

[4]Rasmussen, M. L., "Waverider Configurations Derived from Inclined Circular and Elliptic Cones," *Journal of Spacecraft and Rockets*, Vol. 17, No. 6, 1980, pp. 537–545.

[5]Kim, B. S., Rasmussen, M. L., and Jischke, M. C., "Optimization of Waverider Configurations Generated from Axisymmetric Conical Flows," *Journal of Spacecraft and Rockets*, Vol. 20, No. 5, 1983, pp. 461–469.

[6]Rasmussen, M. L., and Broadway, R. T., "Waverider Configurations Derived from Inclined Circular and Elliptic Cones," AIAA Paper 83–2084, Aug. 1983.

[7]Rasmussen, M. L., and He, X., "Analysis of Cone-Derived Waveriders by Hypersonic Small-Disturbance Theory," NASA 1st International Hypersonic Waverider Symposium, Oct. 1990, pp. 1–46.

[8]Lin, S. C., and Rasmussen, M. L., "Cone-Derived Waverider with Combined Transverse and Longitudinal Curvature," AIAA Paper 88-0371, Jan. 1988.

[9]Hemdan, H. T., and Jischke, M. C., "Inlets for Waveriders Derived from Elliptic-Cone Stream Surfaces," *Journal of Spacecraft and Rockets*, Vol. 24, No. 1, 1987, pp. 23–32.

[10]Lin, S. C., and Luo, Y. S., "Integrated Inlets for Cone-Derived Waveriders with Combined Transverse and Longitudinal Curvature," *Proceedings of the 9th National Conference of the Chinese Society of Mechanical Engineering*, (Taiwan), Vol. 1, Nov. 1992, pp. 229–236.

[11]Emanuel, G., "Waverider Aerodynamics," *Gasdynamics: Theory and Applications*, 1st ed., AIAA Education Series, AIAA, New York, 1986, pp. 399–414.